Polarization-independent adaptive lens with two different blue-phase liquid-crystal layers

Yifan Liu, Yan Li, and Shin-Tson Wu*

CREOL, The College of Optics and Photonics, University of Central Florida, Orlando, Florida 32816, USA

*Corresponding author: swu@ucf.edu

An adaptive microlens structure is proposed using two polymer-stabilized blue-phase liquid-crystal layers whose Kerr constant is largely mismatched. This device exhibits several favorable features, such as polarization independence, simple structure, and good parabolic phase profile. Its applications for 2D/3D switchable displays and other photonic devices are emphasized. © 2013 Optical Society of America

OCIS codes: (110.1080) Active or adaptive optics; (230.3720) Liquid-crystal devices.
http://dx.doi.org/10.1364/AO.52.003216

1. Introduction

Liquid-crystal (LC) adaptive lenses with tunable focal length have found useful applications in autofocusing [1,2], 2D/3D switchable displays [3–6], and tunable photonic devices [7,8]. The majority of such adaptive lenses employ nematic LCs because of their high birefringence, simple alignment, and low operation voltage. However, to achieve a short focal length a relatively thick LC layer ($d \geq 30$ μm) [5,9–11] and high birefringence LC material are needed. For a 30 μm LC layer, its response time is of the order of 1 s [12]. A high-birefringence ($\Delta n > 0.4$) LC helps to reduce cell gap and obtain faster response time, but its ultraviolet (UV) stability is a concern [13]. Moreover, most nematic LC lenses are polarization dependent. To overcome this problem, a straightforward method is to stack two devices in orthogonal directions [14].

Recently, the polymer-stabilized blue-phase LC (BPLC) based on the Kerr effect [15–17] has emerged as an attractive candidate for photonics applications. It exhibits several major advantages: (1) a submillisecond response time [18,19], (2) no need for an alignment layer, and (3) an optically isotropic voltage-off state. In 2010, a hole-patterned microlens using polymer-stabilized BPLC was proposed [20]. The device structure is simple, but the phase profile is not exactly parabolic, and the extraordinary and ordinary polarizations have slightly different focuses because a strong horizontal electric field is generated near the edge of the hole-patterned electrode. In 2011, a polarization-independent blue-phase lens using a curved indium-tin oxide (ITO) electrode was proposed [21], but the fabrication of such structures seems complicated. Moreover, the curved polymer layer shields a portion of the applied voltage because of its small dielectric constant compared to BPLCs. Another BPLC gradient-index lens with planar multielectrodes [22] was proposed to realize a parabolic phase profile at different focal lengths by addressing the pixelated electrodes individually. In this structure, electrodes are easier to fabricate and good image quality can be maintained. However, an additional dielectric layer is needed to shield the unnecessary horizontal field so as to realize polarization insensitivity. To reduce operation voltage, this dielectric layer should have a high dielectric constant, which is not only complicated but also expensive. Moreover, multiple data driving is required to achieve a parabolic lens profile. Recently, a BPLC lens with a resistive film [23] was proposed. Such a lens requires only a single data driving, however, the resistive film

technology on microlens is not mature yet. Some resistive film materials are unstable under strong UV exposure, which plays a key role in the polymerization process of BPLCs. Finally, the concept of a Fresnel lens is also applicable to BPLC material [24]. However, like in all other LC Fresnel lenses [25], it is difficult to generate a sharp 2π phase shift at the edge of each ring in the BPLC Fresnel lens. Therefore, these Fresnel lenses suffer from severe diffraction and multifocus effects, especially at oblique viewing angles and/or under a broadband light source.

In this paper, we propose a new microlens structure using two cascaded polymer-stabilized BPLC layers. The Kerr constant of the first BPLC layer is much larger than that of the second one. Due to the curved interface of the two BPLC layers, optical power is generated. Such a microlens has several attractive features: simple structure, good phase profile, polarization independence under normal incident light, and fast response time. Therefore, it has potential application for 2D/3D switchable displays.

2. Device Structure and Mechanism

Figure 1 depicts the side view of the proposed cylindrical BPLC lens. Sandwiched between top and bottom planar ITO glass substrates are a convex BPLC-1 layer and a concave BPLC-2 layer. BPLC-1 has a similar dielectric constant and refractive index to BPLC-2, but a much smaller Kerr constant. This can be obtained by using the same LC host, but different weight ratios of photocurable monomers and chiral dopant. The following sections will explain in detail the mechanism of well-controlled BPLC recipes affecting the Kerr constant of BPLCs. Both layers of BPLC precursors are cured under UV light for sufficient time to ensure that the polymerization process has been finished. The radius of the lens aperture is R, the central thickness of BPLC-2 is d_1. The edge thickness is d_2, which is also the overall cell gap of the LC layer. In order to reduce the voltage shielding effect, d_1 should be made as small as possible.

When no voltage is applied, there is no optical power because of the matched index between the BPLC layers. Once a voltage is applied between the top and bottom ITO electrodes, uniform vertical electric fields are generated across the lens due to the matched dielectric constant. In BPLC-1, since the
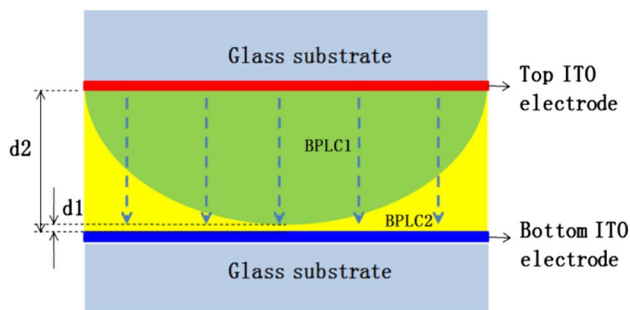
Kerr constant is small, the refractive index change is negligible and the normally incident light sees $n_{\text{ave}} = (2n_o + n_e)/3$. In BPLC-2, a uniform refractive index change occurs across the lens, according to extended Kerr effect [26]:

$$\Delta n_{\text{ind}}(E) = \Delta n_s(1 - exp(-(E/E_s)^2)), \qquad (1)$$

where Δn_s is the saturated induced birefringence of the BPLC composite and E_s is the saturation electric field. Kerr constant K is related to Δn_s and E_s as [26]

$$K = \Delta n_s/(\lambda E_s^2). \qquad (2)$$

The normally incident light experiences a refractive index $n_o = n_{\text{ave}} - \Delta n_{\text{ind}}(E)/3$ in BPLC-2, which decreases with increasing voltage. The phase profile at any radius is calculated based on the optical path lengths in BPLC-1 and BPLC-2. Due to the concave shape and decreased refractive index of the BPLC-2 layer, a phase profile like that of a positive lens is formed.

The dielectric constant matching plays a critical role in this lens design. The first advantage gained from this feature is that the voltage shielding effect is minimized: in this lens design, the voltage drop through the curved BP–BP interface makes a contribution to the lens power, whereas the voltage drop in other layers is a unfavorable shielding effect, such as in the central part of BPLC-2, whose thickness is d_2. Because of the small thickness of d_2 and the dielectric constant matching of BPLC1-BPLC2, only a small portion of voltage is shielded, in contrast to the strong shielding effect on the polymer layer reported in [21]. Another advantage of this design is polarization independence. Because the electrodes are planar and the dielectric constants are matched, uniform vertical electric fields are generated with very small horizontal components. By suppressing the horizontal components, the device is polarization independent [21]. This feature will be quantitatively analyzed in the following sections.

3. Material Preparation and Measurement

We prepared two BPLC mixtures using the same LC host, HTG135200-100 (from HCCH, China) and high twisting power chiral dopant R5011 (from HCCH). The recipes for sample I and sample II are listed in Table 1, where RM257 (Merck) and TMPTA (Sigma Aldrich) are photocurable monomers. The host LC has the following physical properties: $\Delta n = 0.205$ at $\lambda = 642$ nm, $\Delta \varepsilon = 85$ at 1 kHz and 21°C. Different amounts of R5011 were used to control the

Fig. 1. Side view of the proposed adaptive BPLC lens.

Table 1. Recipes of the Employed BPLC Mixtures

	HTG (%)	R5011 (%)	RM257 (%)	TMPTA (%)
Sample I	78.0	10.0	7.2	4.8
Sample II	87.0	5.0	4.8	3.2

pitch length (or Kerr constant) of the two BPLC mixtures.

From Table 1, it can be seen that the weight ratios of photocurable monomers are different in the two samples. For sample I, it is 12 wt. % in total, but for sample II, it is 8 wt. %. This is because the polymer network also plays an important role in the Kerr constant of BPLC materials. A high concentration of the polymer network provides rigid binding to the LC molecules in the double twist cylinder structures, and makes them more difficult to reorient. Macroscopically, this means a smaller Kerr constant. On the other hand, different monomer ratios lead to a slightly mismatched dielectric constant. According to our measurement, the dielectric constant of sample I is $\varepsilon_{ave1} = 25$, and for sample II it is $\varepsilon_{ave2} = 34$. Dielectric mismatching is unfavorable because it generates a horizontal electric field, which in turn degrades the polarization-independence property of the lens. But further simulation in next section will show that such a small mismatch is still acceptable.

In order to measure the Kerr constant of these two samples, we injected the precursors into two vertical field switching (VFS) cells with a 5 μm cell gap [27]. The transition temperature of the precursors between chiral nematic and blue phase during the heating process is 32.7°C for sample I and 68.7°C for sample II. They were cured during the cooling process at 33°C and 70°C, respectively, with an UV light (8 mW/cm²) for 10 min. After the BP mixtures were polymerized, we measured the voltage-dependent transmittance (VT) curves of the two VFS cells using the same method as reported in [27]. The incident angle is 70° and the wavelength is 633 nm. Results are shown in Fig. 2.

The black solid curve represents the VT curve of sample I, and the dashed red curve represents sample II. We can see that the on-state voltage of sample II is ~22 V_{rms}, whereas the peak voltage of sample I is much higher than 40 V_{rms}. This indicates sample II has a much larger Kerr constant than sample I. As discussed before, there are two reasons for this outcome. The first is that, because the Kerr constant is proportional to the square of pitch length [28], the larger concentration of chiral dopant in sample I
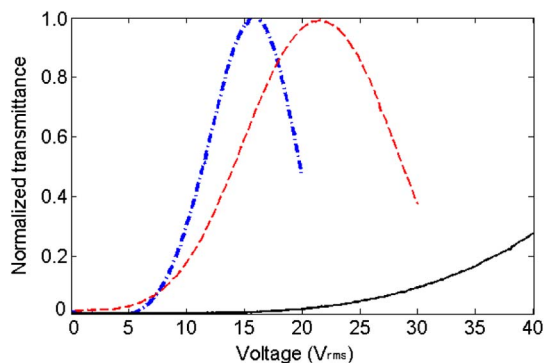
results in a shorter pitch length and a smaller Kerr constant compared to sample II. The second reason is the higher polymer concentration in Sample I, resulting in a more rigid polymer network and lower Kerr constant. After fitting with the extended Kerr model, we obtain the saturation birefringence $\Delta n_{s1} \sim 0.16$ and saturation electric field $E_{s1} = 34.15$ V/μm for sample I and $\Delta n_{s2} \sim 0.18$, $E_{s2} = 11.1$ V/μm for sample II. From Eq. (2), we estimate that the Kerr constant of sample 1 is about 1 order smaller than that of sample 2.

Also included in Fig. 2 (blue dashed–dotted curve) is the VT curve of a JNC JC-BP01M BPLC reported in [29] ($\varepsilon_{ave} = 70$, $\Delta n_{sat} = 0.142$, and $E_s = 4.15$ V/μm). By using this large Kerr constant BPLC composite, the operating voltage is greatly reduced. In order to demonstrate the potential of cascaded BPLC lens design, this JNC material is also used in the simulation (Section 4). We assume that the original JC-BP01M serves as the BPLC-2 of Fig. 1, and BPLC-1 uses another hypothetical BPLC material with the same dielectric constant and Δn_{sat} as BPLC-2, but $E_s = 40$ V/μm.

4. Device Simulation

With the physical properties of BPLC samples in hand, we carried out simulations, first assuming BPLC-1 is HTG sample I, and BPLC-2 is HTG sample II. First, we used the average dielectric constants of BPLC-1 and BPLC-2 to obtain the electric potential distribution using TechWiz. In the simulation, we assume $d_1 = 1$ μm, and $d_2 = 12$ μm. The radius of the microlens is 40 μm, the total BPLC cell gap is 13 μm, and the shape of BPLC-1 is sinusoidal. Figure 3 shows the cross-section view of the cylindrical BPLC lens described above by Fig. 1 and equal-potential lines simulated by TechWiz.

Figure 3 shows an entire lens with a 13 μm cell gap and 80 μm width. It is seen that equal-potential lines are distributed uniformly through the entire cell gap, and primarily in the horizontal direction, implying that the vertical electric field dominates. Actually, the electric field has the strongest horizontal component at point P near the edge of the lens, as shown in Fig. 3. Even at this point, the electric field vector

Fig. 2. VT curves of BPLC samples: black solid curve for sample I, red dashed curve for sample II, and blue dashed–dotted curve for the JNC sample.
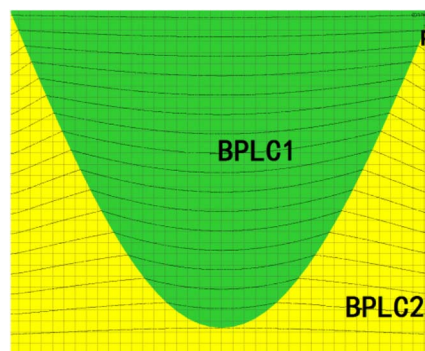

Fig. 3. Cross-section view of BPLC layers: green convex region is sample I and yellow concave region is sample II. Black lines are equal potential lines.

deviates from the vertical direction by only 1.6°. This result proves that the small mismatch of dielectric constants in sample I ($\varepsilon_{ave1} = 25$) and sample II ($\varepsilon_{ave2} = 34$) does not affect the electric field distribution too much.

Then we used the extended Kerr model to calculate the induced birefringence in the BPLC layers and the phase profile across the lens. Figure 4(a) shows the simulated phase profiles using HTG samples at $\lambda = 633$ nm. The driving voltages are 30 V_{rms}, 50 V_{rms}, and 100 V_{rms}. The black solid (o-wave) and blue dashed (e-wave) curves overlap very well, indicating that the lens is polarization independent. This is due to the close match of dielectric constant and uniform vertical electric fields generated along the lens. Moreover, both curves match closely to an ideal parabolic shape, as depicted by the red dotted curves, which means aberration would be suppressed. For comparison, in Fig. 4(b), we show the phase profile of a similar BPLC lens, but the BPLC-1 material is replaced by glass ($\varepsilon = 5$). The severe mismatch of dielectric constant causes much more voltage shielding on the glass layer. Therefore, the phase delay generated by the BPLC deviates from the ideal parabolic
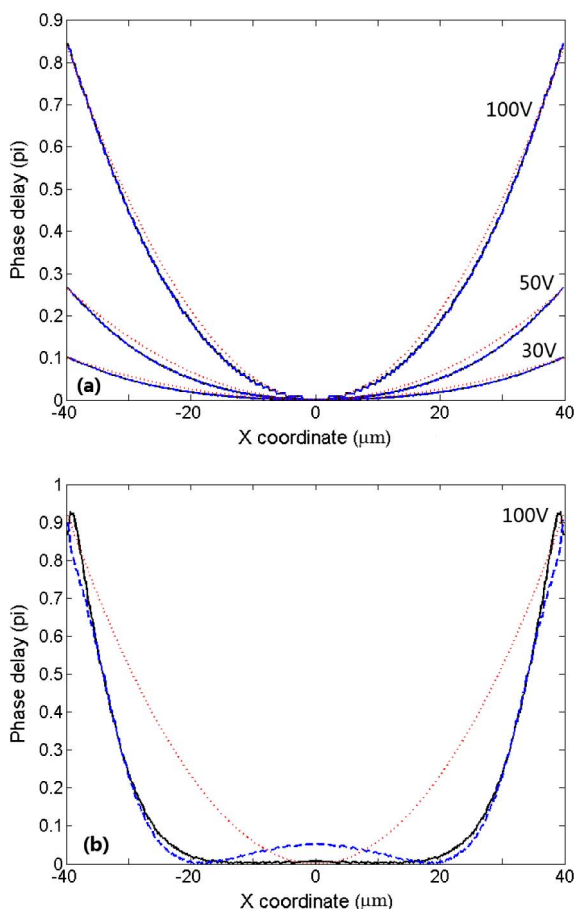
profile significantly. Besides, the o-wave and e-wave profiles separate noticeably, implying that the horizontal field is much stronger than the design shown in Fig. 4(a). As a result, the lens is polarization dependent.

The focal length at different voltages was calculated using $f = R^2 / 2\Delta\Phi(E)$ where $\Delta\Phi(E)$ is the phase difference between the lens center and edge. In Fig. 5, the focal lengths for the o- and e-waves using HTG materials overlap very well, as depicted by the solid black line. To obtain a shorter focal length and lower operational voltage, we also simulated the lens structure using JNC BPLC materials as mentioned in Section 3. Again, the two curves for the o- and e-waves using JCBP01M and the hypothetical BPLC material are indistinguishable, as shown by the dashed blue lines.

Although the simulated results of the proposed BPLC lens are interesting, the device fabrication is challenging. A possible solution is to use a two-step curing process. In the first step, the top substrate is assembled with a parabolic-shaped glass mold to form a LC cell. The BPLC-1 precursor is injected into this cell and UV cured at the BP-I phase. After curing, the BPLC-1 is stabilized and its temperature range broadened significantly. The glass mold is then peeled off, and the planar bottom substrate is assembled. So a chamber is formed between the cured BPLC-1 and the bottom substrate. In the second step, BPLC-2 precursor is injected into this chamber, and cured at the BP-I phase. The curing temperature of BPLC-1 and BPLC-2 may be different, but with the stabilization of the polymer network, the BPLC-1 layer will stay in blue phase at the curing temperature of BPLC-2.

The most challenging step in this fabrication process is to peel off the glass mold without destabilizing the BPLC-1 layer. A possible way is to freeze the sample in liquid nitrogen before peeling off the glass mold. According to our experience, the frozen polymer network is more resistant to the mechanical
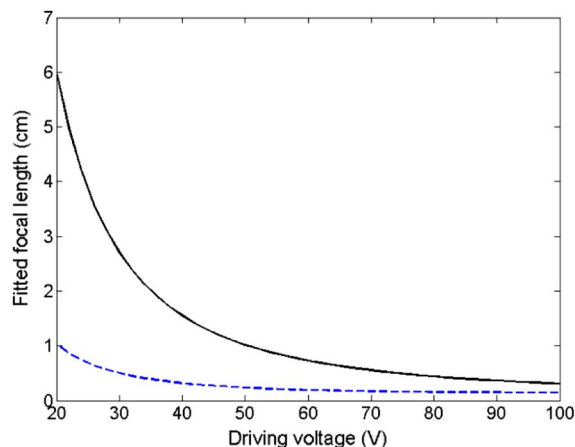

Fig. 4. Phase profiles of the proposed adaptive lens (a) using the HTG samples at 30 V_{rms}, 50 V_{rms}, and 100 V_{rms} and (b) using glass to replace BPLC-1, driven at 100 V_{rms}. Black solid curves are for the o-wave, blue dashed curves are for the e-wave, and red dotted curves are ideal parabolic shapes.

Fig. 5. Voltage-dependent focal length of the BPLC samples: black solid line represents the focal lengths for o- and e-waves using HTG materials, and the blue dotted lines represent JNC materials.

impact incurred during the peeling off process. The LC will be crystallized under low temperature, but it would resume the stabilized blue phase after unfreezing.

5. Conclusion

We have proposed a polarization-independent and fast-response microlens using two polymer-stabilized BPLCs. Due to the curved interface and large Kerr constant difference in the two cascaded BPLC layers, an optical power is generated and can be tuned continuously from infinity to 0.4 cm. Employing the same host LC, the two BPLCs have similar dielectric constants, resulting in less voltage shielding and better polarization independence. The use of planar electrodes and single data driving greatly simplify the fabrication process and driving scheme. With a simple structure, good phase profile, polarization independence under normal incident light, and fast response time, this new microlens has potential applications for autostereoscopic 2D/3D switchable displays.

References

1. S. Sato, "Liquid-crystal lens-cells with variable focal length," Jpn. J. Appl. Phys. **18**, 1679–1684 (1979).
2. C. W. Chen, M. Cho, Y. P. Huang, and B. Javidi, "Three-dimensional imaging with axially distributed sensing using electronically controlled liquid crystal lens," Opt. Lett. **37**, 4125–4127 (2012).
3. M. G. H. Hiddink, S. T. de Zwart, O. H. Willemsen, and T. Dekker, "Locally switchable 3D displays," SID Symp. Dig. Tech. Papers **37**, 1142–1145 (2006).
4. T. Nose, S. Masuda, S. Sato, J. Li, L. C. Chien, and P. J. Bos, "Effect of low polymer content in a liquid crystal microlens," Opt. Lett. **22**, 351–353 (1997).
5. Y. P. Huang, C. W. Chen, and Y. C. Huang, "Superzone Fresnel liquid crystal lens for temporal scanning auto-stereoscopic display," J. Display Technology **8**, 650–655 (2012).
6. L. Lu, L. Shi, P. J. Bos, T. Van Heugten, and D. Duston, "Comparisons between a liquid crystal refractive lens and a diffractive lens for 3D displays," SID Symp. Dig. Tech. Papers **42**, 171–174 (2011).
7. M. Ferstl and A. Frisch, "Static and dynamic Fresnel zone lenses for optical interconnections," J. Mod. Opt. **43**, 1451–1462 (1996).
8. P. F. McManamon, T. A. Dorschner, D. L. Corkum, L. J. Friedman, D. S. Hobbs, M. Holz, S. Liberman, H. Q. Nguyen, D. P. Resler, R. C. Sharp, and E. A. Watson, "Optical phased array technology," Proc. IEEE **84**, 268–298 (1996).
9. Y. Y. Kao, C. P. Chao, and C. W. Hsueh, "A new low-voltage-driven GRIN liquid crystal lens with multiple ring electrodes in unequal widths," Opt. Express **18**, 18506–18518 (2010).
10. Y. H. Fan, H. W. Ren, X. Liang, H. Wang, and S. T. Wu, "Liquid crystal microlens arrays with switchable positive and negative focal lengths," J. Display Technology **1**, 151–156 (2005).
11. B. Wang, M. Ye, and S. Sato, "Liquid crystal lens with focal length variable from negative to positive values," IEEE Photon. Technol. Lett. **18**, 79–81 (2006).
12. H. Ren, D. Fox, B. Wu, and S. T. Wu, "Liquid crystal lens with large focal length tunability and low operating voltage," Opt. Express **15**, 11328–11335 (2007).
13. S. Gauza, H. Wang, C. H. Wen, S. T. Wu, A. Seed, and R. Dabrowski, "High birefringence isothiocyanato tolane liquid crystals," Jpn. J. Appl. Phys. **42**, 3463–3466 (2003).
14. Y. H. Lin, H. Ren, Y. H. Wu, Y. Zhao, J. Fang, Z. Ge, and S. T. Wu, "Polarization-independent liquid crystal phase modulators using a thin polymer-separated double-layered structure," Opt. Express **13**, 8746–8752 (2005).
15. H. Kikuchi, M. Yokota, Y. Hisakado, H. Yang, and T. Kajiyama, "Polymer-stabilized liquid crystal blue phases," Nat. Mater. **1**, 64–68 (2002).
16. Y. Haseba, H. Kikuchi, T. Nagamura, and T. Kajiyama, "Large electro-optic Kerr effect in nanostructured chiral liquid-crystal composites over a wide temperature range," Adv. Mater. **17**, 2311–2315 (2005).
17. Z. Ge, S. Gauza, M. Jiao, H. Xianyu, and S. T. Wu, "Electro-optics of polymer-stabilized blue phase liquid crystal displays," Appl. Phys. Lett. **94**, 101104 (2009).
18. K. M. Chen, S. Gauza, H. Xianyu, and S. T. Wu, "Submillisecond gray-level response time of a polymer-stabilized blue phase liquid crystal," J. Display Technology **6**, 49–51 (2010).
19. Y. Chen, J. Yan, J. Sun, S. T. Wu, X. Liang, S. H. Liu, P. J. Hsieh, K. L. Cheng, and J. W. Shiu, "A microsecond-response polymer-stabilized blue phase liquid crystal," Appl. Phys. Lett. **99**, 201105 (2011).
20. Y. H. Lin, H. S. Chen, H. C. Lin, Y. S. Tsou, H. K. Hsu, and W. Y. Li, "Polarizer-free and fast response microlens arrays using polymer-stabilized blue phase liquid crystals," Appl. Phys. Lett. **96**, 113505 (2010).
21. Y. Li and S. T. Wu, "Polarization independent adaptive microlens with a blue-phase liquid crystal," Opt. Express **19**, 8045–8050 (2011).
22. C. T. Lee, Y. Li, H. Y. Lin, and S. T. Wu, "Design of polarization independent multi-electrode GRIN lens with a blue-phase liquid crystal," Opt. Express **19**, 17402–17407 (2011).
23. Y. Li, Y. Liu, Q. Li, and S. T. Wu, "Polarization independent blue-phase liquid crystal cylindrical lens with a resistive film," Appl. Opt. **51**, 2568–2572 (2012).
24. C. H. Lin, Y. Y. Wang, and C.-W. Hsieh, "Polarization-independent and high-diffraction-efficiency Fresnel lenses based on blue phase liquid crystals," Opt. Lett. **36**, 502–504 (2011).
25. Y. H. Fan, H. Ren, and S. T. Wu, "Switchable Fresnel lens using polymer-stabilized liquid crystal," Opt. Express **11**, 3080–3086 (2003).
26. J. Yan, H. C. Cheng, S. Gauza, Y. Li, M. Jiao, L. Rao, and S. T. Wu, "Extended Kerr effect of polymer-stabilized blue-phase liquid crystals," Appl. Phys. Lett. **96**, 071105 (2010).
27. H. C. Cheng, J. Yan, T. Ishinabe, and S. T. Wu, "Vertical field switching for blue-phase liquid crystal devices," Appl. Phys. Lett. **98**, 261102 (2011).
28. P. R. Gerber, "Electro-optical effects of a small-pitch blue-phase system," Mol. Cryst. Liq. Cryst. **116**, 197–206 (1985).
29. L. Rao, J. Yan, S. T. Wu, S. Yamamoto, and Y. Haseba, "A large Kerr constant polymer-stabilized blue phase liquid crystal," Appl. Phys. Lett. **98**, 081109 (2011).